HHS Public Access

Author manuscript

Nat Neurosci. Author manuscript; available in PMC 2020 November 01.

Published in final edited form as:

Nat Neurosci. 2020 May ; 23(5): 615–624. doi:10.1038/s41593-020-0619-5.

Reduced C9ORF72 function exacerbates gain-of-toxicity from ALS/FTD-causing repeat expansion in *C9orf72*

Qiang Zhu[1,14], **Jie Jiang**[1,2,14], **Tania F. Gendron**[3], **Melissa McAlonis-Downes**[1], **Lulin Jiang**[4], **Amy Taylor**[5], **Sandra Diaz Garcia**[5], **Somasish Ghosh Dastidar**[6,7], **Maria J. Rodriguez**[5], **Patrick King**[1], **Yongjie Zhang**[3], **Albert R. La Spada**[6,8], **Huaxi Xu**[4], **Leonard Petrucelli**[3], **John Ravits**[5], **Sandrine Da Cruz**[1,9,10], **Clotilde Lagier-Tourenne**[11,12,15], **Don W. Cleveland**[1,5,13,15]

[1]Ludwig Institute for Cancer Research, University of California at San Diego, La Jolla, California, USA

[2]Department of Cell Biology, Emory University School of Medicine, Atlanta, Georgia, USA

[3]Department of Neuroscience, Mayo Clinic, 4500 San Pablo Road, Jacksonville, Florida, USA

[4]Neuroscience Initiative, Sanford Burnham Prebys Medical Discovery Institute, La Jolla, California, USA

[5]Department of Neurosciences, University of California at San Diego, La Jolla, California, USA

[6]Department of Pediatrics, University of California at San Diego, La Jolla, California, USA

[7]Current address: Molecular Neuroscience; Kasturba Medical College; Manipal academy of Higher Education, Manipal, India

[8]Departments of Neurology, Neurobiology, and Cell Biology, Duke Center for Neurodegeneration and Neurotherapeutics, Duke University School of Medicine, Durham, North Carolina, USA

[9]VIB Center for Brain and Disease Research, Leuven, Belgium

[10]Department of Neurosciences, KU Leuven, Leuven, Belgium

[11]Department of Neurology, The Sean M. Healey and AMG Center for ALS at Mass General, Massachusetts General Hospital, Harvard Medical School, Boston, Massachusetts, USA

[12]Broad Institute of Harvard University and MIT, Cambridge, Massachusetts, USA

[13]Department of Cellular and Molecular Medicine, University of California at San Diego, La Jolla, California, USA

[14]These authors contributed equally

Abstract

[15]To whom correspondence should be addressed: dcleveland@ucsd.edu or clagier-tourenne@mgh.harvard.edu.

AUTHOR CONTRIBUTIONS

Q.Z., J.J., S.D.C., C.L.-T. and D.W.C. designed research; Q.Z., J.J., T.F.G., A.R.L.S., H.X., L.P., J.R., S.D.C., C.L.-T. and D.W.C analyzed the data; Q.Z., J.J., T.F.G., M.M.D., L.J., A.T., S.D.G., S.G.D., M.J.R., P.K., and Y.Z. performed research; Q.Z., J.J., S.D.C., C.L.-T. and D.W.C. wrote the manuscript.

COMPETING FINANCIAL INTERESTS

D.W.C. is a consultant for Ionis Pharmaceuticals. The other authors report no conflict of interest.

Hexanucleotide expansions in *C9orf72* are the most frequent genetic cause of amyotrophic lateral sclerosis (ALS) and frontotemporal dementia (FTD). While repeat expansion has been established to generate toxic products, mRNAs encoding the C9ORF72 protein, a predicted guanine exchange factor, are also reduced in affected individuals. We now test how C9ORF72 protein levels affect repeat-mediated toxicity. In somatic transgenic mice expressing 66 GGGGCC repeats, inactivation of one or both endogenous *C9orf72* alleles provokes or accelerates, respectively, early death. In mice expressing a *C9orf72* transgene with 450 repeats that does not encode the C9ORF72 protein, inactivation of one or both endogenous *C9orf72* alleles exacerbates cognitive deficits, hippocampal neuron loss, glial activation, and accumulation of dipeptide-repeat proteins from translation of repeat-containing RNAs. Reduced C9ORF72 is shown to suppress repeat-mediated elevation in autophagy. These efforts suggest a disease mechanism in ALS/FTD resulting from reduced C9ORF72 producing autophagy deficits that synergize with repeat-dependent gain-of-toxicity.

INTRODUCTION

Hexanucleotide (GGGGCC) expansion in a noncoding region of the *C9orf72* gene is implicated in the largest proportion of familial amyotrophic lateral sclerosis (ALS) and frontotemporal dementia (FTD), as well as in approximately 10% of instances of sporadic ALS[1, 2]. While normal individuals have less than 25 GGGGCC repeats, this repeat has been expanded to hundreds and can somatically expand further to thousands in parts of the nervous system of individuals with *C9orf72*-mediated ALS/FTD (referred to hereafter as C9ALS/FTD). The finding of *C9orf72* repeat expansion as causative of both ALS and FTD, two devastating adult-onset neurodegenerative diseases with distinct clinical features, provoked hypotheses for disease mechanism that include “gain-of-toxicity” or reduction in function of the C9ORF72 protein, a predicted guanine exchange factor (GEF) for one or more as yet unidentified G protein(s)[3].

The most frequently proposed gain-of-toxicity is from accumulation of aberrant dipeptide-repeat (DPR) proteins encoded by repeat-containing RNAs that may be produced through repeat-associated non-AUG-dependent (RAN) translation, an unconventional translation initiation first detected by Ranum and colleagues in spinocerebellar ataxia type 8 and myotonic dystrophy[4]. In C9ALS/FTD patients, the bidirectionally transcribed pathogenic repeat expansion can be translated into five poly-dipeptides (DPRs) [poly(GA), poly(GR), poly(GP), poly(PA), and poly(PR)] depending on the reading frame and direction of RNA transcription. Aggregates of these DPR proteins, which recruit p62, an adaptor protein thought to mediate selective autophagy, have repeatedly been detected in postmortem tissues from C9ALS/FTD patients[5–7]. Several groups have reported that C9ORF72 DPR proteins are toxic *in vivo* and *in vitro (see review*[8]), although, in most studies, rapidly developing toxicity was driven by exposing cells to high extracellular levels of short dipeptides or using AUG-dependent translation in model organisms accumulating high to extraordinary levels of one or more DPR proteins in their nervous system.

The arginine-containing DPR proteins [poly(GR) and poly(PR)] are apparently the most toxic, and were reported to damage nucleolar structure and RNA processing when

exogenously added to cell cultures or expressed at high level in cultured neurons, and can cause severe neurodegeneration when expressed at high levels in *Drosophila*, zebrafish, *C. elegans*, or mice[8]. Poly(GA) is the most abundantly accumulated DPR protein in patients[9] and can be neurotoxic when expressed in cultured cells, the mouse central nervous system (CNS), or zebrafish[8]. Poly(GP) and poly(PA) seem to be more tolerated. Notably, poly(GR) and poly(PR) were reported to interact with proteins with low complexity domains and to alter their phase separation, leading to perturbed assembly, dynamics and function of membrane-less organelles, including stress granules, nucleoli, nuclear pores and spliceosomes[8]. As reported for other aggregation-prone proteins[10], accumulated DPR proteins have consistently been linked to nucleocytoplasmic transport defects. While some reports proposed that poly(GA)[9] and poly(GR)[11] are associated with clinically relevant areas such as the frontal cortex, other examinations of postmortem samples from individuals with an expansion in *C9orf72* failed to find a correlation between neurodegeneration and the amount and/or distribution of DPR protein pathology[12].

An alternative possible gain-of-toxicity mechanism depends on sense or antisense RNAs forming nuclear and/or cytoplasmic repeat-containing RNA foci, a hallmark feature found in C9ALS/FTD patient tissues[1, 5, 6, 13]. Such foci are proposed to sequester RNA-binding proteins and splicing factors and thus cause RNA processing alterations, a mechanism described in other nucleotide repeat expansion diseases including myotonic dystrophy[14]. Several candidates were reported to bind GGGGCC repeats or foci in *C9orf72* diseases, including RanGap1, ADARB2, nucleolin, hnRNP-H, hnRNPA1, hnRNPA3, ASF/SF2, Pur-α, Zfp106, SRSF2, ALYREF and hnRNP H1/F (see review[15]). RNA foci were also reported in the cytoplasm or neurites[16]. While several studies failed to identify *C9orf72* repeat RNA foci toxicity in flies, toxicity from repeat RNAs without detectable DPR protein accumulation has been reported in primary neurons, chick embryonic spinal cord and zebrafish[15].

Multiple efforts using germline or somatic transgenesis of GGGGCC repeats in mice demonstrated a repeat-dependent gain-of-toxicity that can drive DPR proteins and RNA foci accumulation accompanied by ALS/FTD-related neurodegenerative phenotypes[17–19]. Added to this, examination of patient tissues produced a consensus that the repeat expansion decreases levels of the *C9orf72* mRNA[1, 20, 21] and protein[11, 22, 23], reductions that correlate with histone and DNA hypermethylation near and within the expanded repeat[20, 24, 25]. While loss of C9ORF72 in zebrafish[26] and *C. elegans*[27] was reported to produce motor deficits, reduction or elimination of C9ORF72 in mice is not associated with neurodegeneration but rather with shortened life span from age-dependent abnormalities outside of the nervous system, including splenomegaly and enlarged cervical lymph nodes[17,28–32]. Consistent with this, elimination of C9ORF72 selectively from neurons and glia did not cause motor neuron degeneration, motor dysfunction, or disease in mice[33]. However, compared to human motor neurons produced from pluripotent stem cells (iPSCs) from normal individuals, iPSC-derived motor neurons generated from *C9orf72* patients or harboring a CRISPR/Cas9-mediated *C9orf72* deletion were found to undergo more rapid neurodegeneration in response to withdrawal of neurotrophic factors and/or transient exposure to high levels of glutamate[34].

The function of the C9ORF72 protein is not established, although accumulating evidence suggests that it functions in a complex with the WDR41 and SMCR8 proteins, which together have been reported to produce GEF activity for Rab8a and Rab39b[32, 35]. C9ORF72 is proposed to function (directly or indirectly) in control of autophagic flux[30, 32, 35, 36] and/or endosomal trafficking[35, 37, 38]. Whatever its actual role(s), a key unresolved question is whether reduced production of the C9ORF72 protein from the affected allele synergizes with a gain-of-toxicity from expression of the repeat expansion to drive age-dependent ALS and/or FTD in the mammalian nervous system. We now test this in cohorts of mice in which neither, one, or both endogenous *C9orf72* alleles are inactivated and which express transgenes encoding either 66 GGGGCC repeats or a 450 GGGGCC repeat-containing *C9orf72* gene that does not encode the 54 kD C9ORF72 protein.

RESULTS

Reduction or absence of C9ORF72 in mice expressing 66 GGGGCC repeats accelerates premature death and DPR protein accumulation

We first assessed potential damage conferred on motor neurons from loss of C9ORF72 function by taking advantage of mouse embryonic stem cells containing a GFP transgene under the control of a murine motor neuron specific Hb9 promoter. After differentiation, Hb9::GFP+ mouse motor neurons were sorted and treated with antisense oligonucleotides (ASOs) that when hybridized to the *C9orf72* RNAs would trigger their RNase H-mediated degradation (Supplementary Fig. 1a). Within two weeks of C9-ASO treatment, endogenous *C9orf72* RNAs were reduced more than 50% (Supplementary Fig. 1b). Similar to a report that neuronal morphology, including dendritic arborization and spine density, is significantly altered in primary hippocampal neurons isolated from *C9orf72* knockout mice[39], reduction in *C9orf72* RNAs produced a >50% reduction in neurite outgrowth compared to motor neurons differentiated in parallel and treated with a scrambled sequence ASO (Supplementary Fig. 1c). Although reduction or elimination of C9ORF72 is not sufficient to cause neurodegeneration in mice[17,28–33], this *in vitro* study demonstrates that reduced C9ORF72 can affect the normal growth and morphology of motor neurons and potentially makes them more vulnerable to other insults.

To directly test whether reduction in C9ORF72 function synergizes with repeat-mediated gain-of-toxicity to exacerbate disease within the mammalian nervous system, we first used somatic transgenesis with adeno-associated virus (AAV) to express either 2 or 66 GGGGCC repeats (C9AAV)[19]. Either AAV was injected intracerebroventricularly into post-natal day 0 mice in which neither, one, or both endogenous *C9orf72* alleles were inactivated (Fig. 1a). Two weeks after injection, the repeat transgene was highly expressed in the cortex, with much lower levels detected in the cerebellum and spinal cord (Supplementary Fig. 2a). Cortical accumulation of 66 repeat-containing RNAs was not affected by reduction or elimination of endogenous C9ORF72 protein (Supplementary Fig. 2b). No transgene expression was detectable in peripheral tissues including spleen (Supplementary Fig. 2a).

Mice injected with C9AAV expressing either 2 or 66 GGGGCC repeats and with complete loss of C9ORF72 ($C9^{2R}$,$C9orf72^{-/-}$ and $C9^{66R}$,$C9orf72^{-/-}$) had shortened lifespans relative to the corresponding C9AAV-injected mice with one or both endogenous *C9orf72* alleles

intact (Fig. 1b). Absence of C9ORF72 in $C9^{2R}$ and $C9^{66R}$ mice was accompanied by development of enlarged spleens (Supplementary Fig. 2c), as initially reported in *C9orf72*$^{-/-}$ mice[17]. The combination of C9ORF72 complete loss of function with expression of 66 repeats accelerated death by 2 months relative to mice injected with 2-repeat containing C9AAV ($C9^{66R}$,*C9orf72*$^{-/-}$, 225 ± 12 days vs. $C9^{2R}$,*C9orf72*$^{-/-}$, 284 ± 18 days) (Fig. 1b). Extensive postmortem examination of central nervous system or peripheral tissues revealed similar splenomegaly in $C9^{2R}$,*C9orf72*$^{-/-}$ and $C9^{66R}$,*C9orf72*$^{-/-}$ mice (Supplementary Fig. 2c), but did not uncover the basis for accelerated death in the 66 repeat injected *C9orf72* null mice.

More strikingly, while injection of C9AAV expressing 66 repeats into mice with normal C9ORF72 function did not significantly affect lifespan, expression of the 66 repeats combined with 50% reduction in endogenous *C9orf72* – mimicking what is observed in the affected regions of C9-ALS/FTD patients[1, 11, 20–25, 40] – drove sudden, premature deaths that were not observed in *C9orf72*$^{+/-}$ mice expressing 2 repeats (Fig. 1b). Detailed examination of major organs in 15-month-old *C9orf72*$^{+/-}$ mice expressing either 2 repeats or 66 repeats did not reveal significant differences beyond the accumulation of repeat encoded DPRs in cortex and hippocampus of 66 repeat mice (see below). Regardless, the accelerated death in 66 repeat somatic transgenic mice when C9ORF72 levels are reduced or eliminated offers strong support for a synergistic combination of damage from gain of repeat toxicity and loss of C9ORF72 function.

Mice expressing 66 repeats accumulated abundant poly(GA) aggregates in the hippocampal region, consistent with the previous report[19]. Most aggregated inclusions were globular in shape and localized intranuclearly in 3-month-old mice (Fig. 1c, left). By 10 months, many inclusions had converted into large, cytoplasmic, ring-like aggregates in cells of the hippocampus (Fig. 1c, right). As in patient tissues[6], most DPR aggregates were p62-positive in mice either with normal or reduced C9ORF72 (Fig. 1c). There was an age-dependent increase (from 12% at 3 months to 31% at 10 months) in the percentage of hippocampal CA1 neurons containing poly(GA) aggregates (Fig. 1d) in $C9^{66R}$,*C9orf72*$^{+/+}$ mice, and similar age-dependent increase was observed for poly(GR) aggregates (Fig. 1e). Reduction or loss of C9ORF72 accelerated initial accumulation of poly(GA) and poly(GR), with the fraction of cells with DPR aggregates increasing as C9ORF72 was reduced (Fig. 1d,e). The average size of poly(GA) aggregates significantly increased in 10-month-old mice with reduced endogenous C9ORF72 (Fig. 1c,f).

Aggregated DPRs in mice expressing 66 repeats were accompanied by a trend in accelerated accumulation of soluble DPRs (as measured by poly(GP) and poly(GA) immunoassays of 2% SDS-soluble homogenates from cortex of 3-month-old mice; Supplementary Fig. 2d,e) in mice with normal, reduced, or no C9ORF72 protein. The accumulation of SDS-soluble DPRs also showed an age-dependent pattern with poly(GP) and poly(GA) increasing ~5-fold from 3 to 10 months of age, reaching ~0.5% and 1%, respectively, of total brain protein, independent of the C9ORF72 protein level (Supplementary Fig. 2d,e).

C9orf72 BAC transgenic mice do not accumulate human C9ORF72 protein

Previously, we have established multiple mouse lines carrying a bacterial artificial chromosome (BAC) containing a human *C9orf72* gene with a repeat expansion. With these, we demonstrated an expression level and repeat number dependent expansion-mediated "gain-of-toxicity" that can provoke repeat-containing RNA foci, DPR translation products, and age-dependent cognitive disease[17]. We extended our initial test of potential synergy between *C9orf72* loss of function and gain-of-toxicity using one of these BAC transgenic lines that expresses 450 repeats at a physiologically relevant level[17].

The BAC transgene contains 140 kb of sequences 5' upstream of the *C9orf72* transcription initiation site (Fig. 2a), including what is predicted to be the complete promoter region and exons 1–5 of the *C9orf72* gene. This *C9orf72* transgene does not encode the 54 kD full length C9ORF72 protein; however, it does carry the sequences which could encode a predicted 222 amino acid, 25 kD short isoform of C9ORF72[1]. The full length C9ORF72 protein belongs to the DENN (differentially expressed in neoplastic versus normal cells) protein family whose known functions are as GEFs for the Rab family of G proteins[3, 41]. The DENN proteins consist of three parts (Fig. 2b): the original DENN domain (DENN) and more divergent domains called uDENN (upstream DENN) and dDENN (downstream DENN). All three domains are implicated in GEF activity.

Recognizing that the predicted short C9ORF72 isoform contains the uDENN and the first third of the DENN domain (Fig. 2b), and the possibility that it may function as a GEF (alone or with partners), we determined whether this predicted 25 kD C9ORF72 isoform accumulated in our $C9^{450C}$ transgenic mice and if so, to what extent relative to normal level of full length C9ORF72. For quantitation standards, His-tagged full length and short C9ORF72 polypeptides were expressed in bacteria and purified (Fig. 2c). When the recombinant proteins were added to brain extracts from *C9orf72* null mice, the recombinant 25 kD isoform and full length C9ORF72 proteins were recognized on immunoblots developed with an antibody generated to the amino terminal 169 residues of C9ORF72, and predicted to bind full length or truncated C9ORF72 isoforms with equal affinity (Fig. 2d).

As expected, endogenous, full length C9ORF72 was identified to be at equivalent levels in extracts of cortex from either non-transgenic or $C9^{450C}$ mice and was undetectable in extracts from *C9orf72*$^{-/-}$ mice (Fig. 2e). No predicted short isoform C9ORF72 was detected in any mouse genotype (Fig. 2e) or in extracts of normal human frontal cortex (Fig. 2d). Using dilutions of recombinant proteins, we determined that the 25 kD C9ORF72 short isoform, if produced at all, is accumulated to less than 4% and 2% (our detection limits) of the level of full length C9ORF72 protein in normal human brain or non-transgenic mice, respectively (Fig. 2e; Supplementary Fig. 3). Thus, the $C9^{450C}$ mice, although generating an RNA level around 4 times the normal level of endogenous mouse *C9orf72* mRNA[17], do not accumulate detectable levels of either the full length or predicted short isoform of the human C9ORF72 protein.

Reduction or loss of C9ORF72 exacerbates cognitive and motor deficits in *C9orf72* BAC transgenic mice

To determine how reduction in C9ORF72 affects toxicity from expression of a GGGGCC repeat expansion, we employed a strategy using two rounds of mating of $C9^{450C}$ mice to mice with inactivation of one or both endogenous *C9orf72* alleles[17] (Fig. 3a). $C9^{450C}$ mice with neither, one, or two inactivated endogenous *C9orf72* alleles (designated as $C9^{450C}$, $C9^{450C}$,*C9orf72*$^{+/-}$ and $C9^{450C}$,*C9orf72*$^{-/-}$, respectively) were born in ratios near that expected for Mendelian inheritance (Fig. 3a). All mice were in a C57BL/6 genetic background, thereby limiting potential confounding influences from other genetic differences.

To determine whether reduction or complete loss of C9ORF72 triggered or exacerbated cognitive and/or motor deficits in mice expressing 450 hexanucleotide repeats, longitudinal behavioral assessments were performed in $C9^{450C}$ mice with neither, one, or both endogenous *C9orf72* alleles inactivated (Fig. 3, Supplementary Fig. 4). By 12 months of age mice with both endogenous *C9orf72* alleles inactivated, with or without the $C9^{450C}$ transgene, developed peripheral phenotypes including enlarged cervical lymph nodes and splenomegaly (Fig. 3b,c) despite total body weight being indistinguishable with or without the $C9^{450}$ transgene (Supplementary Fig. 4a). Survival curves of *C9orf72*$^{-/-}$ mice with or without the $C9^{450C}$ transgene were also indistinguishable (Fig. 3d), with both genotypes developing premature death, evidence further supporting that the BAC $C9^{450C}$ transgene does not generate a functional C9ORF72 protein product that is able to rescue the phenotypes arising from inactivating the endogenous alleles in mice.

While performance of young mice was indistinguishable across all genotypes, $C9^{450C}$ mice developed age-dependent learning and memory deficits by 12 months of age (Fig. 3e), making more errors compared to their non-transgenic littermates in spatial learning and memory tasks (as we had previously reported[17]). Partial or complete removal of endogenous C9ORF72 exacerbated this age-dependent impairment (Fig. 3e). Reduction or complete loss of C9ORF72 by itself did not cause similar behavioral deficits (Fig. 3e). Remarkably, while the $C9^{450C}$ mice did not lose grip strength or develop motor neuron disease at any age (Supplementary Fig. 4b - consistent with our previous report[17]), $C9^{450C}$ mice with partial or complete loss of C9ORF72 developed age-dependent deficits in coordinated motor skills that initiated by 6 months of age and persisted up to the oldest ages examined (Fig. 3f). In addition, $C9^{450C}$ mice with complete loss of endogenous C9ORF72 showed trends of abnormal stride length (Supplementary Fig. 4c) and reduced general activity (Supplementary Fig. 4d). These results identify synergism of C9ORF72 loss of function and gain-of-toxicity from *C9orf72* GGGGCC repeat expansion in provoking abnormalities in coordinated motor skills, which are dependent on both motor neuron/muscle function and cognitive function(s) of other brain regions, including hippocampus[42].

Reduced C9ORF72 exacerbates hippocampal neuronal loss and glial activation in $C9^{450C}$ mice

As the hippocampus plays an important role in spatial learning and memory, we examined whether reduction or elimination of endogenous C9ORF72 affected the age-dependent

hippocampal neuron loss previously observed in the CA1 and dentate gyrus regions of $C9^{450C}$ mice[17]. By 12 months of age, complete loss of C9ORF72 in $C9^{450C}$ mice significantly increased hippocampal neuronal loss (Fig. 4a,b), accompanied by increased activation of microglia and astrocytes (Fig. 4c,d). Deficits of coordinated motor skills and motor learning ability in $C9^{450C}$ mice with reduced endogenous C9ORF72 (Fig. 3f) were not accompanied by loss or decreased cellular size of ChAT-positive lumbar motor neurons (Fig. 4e,f; Supplementary Fig. 5a) or degeneration of motor axons (Supplementary Fig. 5b–d). In addition, no significant astrogliosis or microgliosis was observed at 12 months of age in spinal cords of $C9^{450C}$ mice with partial or complete loss of C9ORF72 (Supplementary Fig. 5e). These results indicate that the motor deficits observed in $C9^{450C}$ mice with reduced endogenous C9ORF72 do not result from degeneration of spinal motor neurons, but are likely to arise from dysfunction of brain regions implicated in motor activity.

Reduction in C9ORF72 exacerbates DPR protein accumulation in $C9^{450C}$ mice

The $C9^{450C}$ transgenic mice accumulate DPR proteins in multiple CNS regions[17], a neuropathological hallmark of C9ALS/FTD[5–7], with SDS soluble DPRs in their cortex present at a level ~300 times lower than that observed in the C9AAV somatic transgenic animals (Supplementary Fig. 5f). Loss of endogenous C9ORF72 did not affect the accumulation of the $C9^{450C}$ repeat-containing RNA (Fig. 5a), confirming that the original DPR production is likely to be similar across all transgenic experimental groups. Nevertheless, by 6 months of age reduction in C9ORF72 accelerated accumulation of 2% SDS soluble poly(GP) and poly(GA) in the cortex (Fig. 5b,c). This increase in poly(GP) and poly(GA) was C9ORF72 dose-dependent, with higher levels accumulating in $C9^{450C}$ mice with complete absence of endogenous C9ORF72 ($C9^{450C}$,*C9orf72*$^{-/-}$) (Fig. 5b,c). Furthermore, loss of C9ORF72 led to an increased frequency of cells accumulating poly(GA) aggregates in the retrosplenial granular cortex of 6 month old $C9^{450C}$ mice (Fig. 5d,e).

Reduction of C9ORF72 in $C9^{450C}$ mice decreases autophagy

Accumulating evidence has implicated disrupted autophagy, a cellular process to clear aberrant proteins, as a component contributing to loss of neurons in various neurodegenerative diseases[43]. Recognizing that C9ORF72 has been proposed to participate in autophagy[35, 37, 39], we examined how reduction or loss of C9ORF72 affected autophagy in non-transgenic or $C9^{450C}$ mice. We initially focused on levels of the central autophagy protein LC3B-I and its autophagosomal membrane bound isoform LC3B-II, the latter produced by lipidation of the former as an intermediate of active autophagy and widely used as an indicator of autophagic activation[44]. Under basal culture conditions and treatment with bafilomycin A1 (an inhibitor of the vacuolar H+ ATPase that prevents the fusion of autophagosomes with lysosomes and disrupts autophagic flux) or rapamycin (a blocker of the mammalian target of rapamycin (mTOR) signaling that induces autophagy), accumulated levels of LC3B-II were decreased in mouse ear fibroblast (MEF) cells isolated from adult mice with reduced or complete loss of C9ORF72 (Supplementary Fig. 6a,b), consistent with suppressed autophagy function.

Cortical levels of LC3B-I and LC3B-II and p62, an ubiquitin-binding scaffold protein thought to function in targeting ubiquitinated proteins to autophagosomes for degradation[44], were not changed in non-transgenic mice with reduced C9ORF72 (Supplementary Fig. 6c,d), evidence supporting that C9ORF72 reduction alone does not affect baseline autophagy. In $C9^{450C}$ mice with normal levels of C9ORF72 both LC3B-I and LC3B-II were elevated relative to non-transgenic mice, suggesting that DPR proteins encoded by repeat-containing RNAs drive increased autophagy (Fig. 5f,g). Remarkably, reduction or loss of endogenous C9ORF72 suppressed this hexanucleotide repeat-mediated induction of both LC3B-I and LC3B-II (Fig. 5f,g). In addition, the magnitude of protein ubiquitination was not altered in non-transgenic or $C9^{450C}$ mice with reduced C9ORF72 level (Supplementary Fig. 6e), showing no obvious compromise of the ubiquitin proteasome system, another highly regulated mechanism of intracellular protein degradation[45].

DISCUSSION

We employed two strategies to determine whether loss of C9ORF72 activity exacerbates gain-of-toxicity from GGGGCC repeat expansion in the *C9orf72* gene. Using AAV9-driven somatic transgenesis in mice expressing a high level of a short repeat expansion or germline transgenics expressing a lower level of a longer repeat, we identified that reduction or absence of the C9ORF72 protein suppresses repeat-mediated elevation in autophagy while enhancing 1) activation of glial cells, 2) early accumulation of DPR proteins, 3) cognitive deficits, and 4) hippocampal neuron degeneration. Strikingly, high expression of 66 repeats provoked or significantly accelerated, respectively, early death in mice with reduced or complete loss of C9ORF72. These efforts provide direct support for disease mechanism in ALS/FTD from reduced C9ORF72 function synergizing with repeat-dependent gain-of-toxicity (Supplementary Fig. 7).

How might loss of C9ORF72 protein function exacerbate gain of toxicity at the cellular and molecular level? C9ORF72 shares sequence homology with the DENN protein family and is thus predicted to be a GEF for as yet unidentified small G protein(s)[3, 41]. C9ORF72 has also been implicated in autophagy[30, 35–37,39], albeit there is no agreement on which step(s) is(are) affected. Evidence from one group supports an interaction of C9ORF72 with Rab1a and the ULK1 complex that act in regulating autophagy initiation[37]. Other evidence supports that C9ORF72 forms a complex with the WDR41 and SMCR8 proteins, which together have GEF activity for RAB8a and RAB39b, and function to control autophagic flux[32, 35, 36]. Another study reported a C9ORF72 interaction with SMCR8, but reported that loss of C9ORF72 inhibited mTOR signaling and enhanced autophagy flux[30]. An additional recent study found that C9ORF72 associates with p62 and may be involved in eliminating stress granules through autophagy[46]. Adding to this prior work, our results demonstrate that in the mouse CNS reduction or loss of C9ORF72 leads to an accelerated accumulation of DPR proteins from a repeat-expressing *C9orf72* germline transgene or from an AAV9-encoded, somatic transgene carrying 66 repeats Figs. 1 and 5).

Our evidence is consistent with the notion that C9ORF72 promotes autophagy in the CNS. Indeed, we document that reduction or loss of C9ORF72 prevents $C9^{450C}$ transgene-mediated autophagic induction (measured by increases in both total LC3B and its active

isoform) (Fig. 5f,g). The consequence of reduced autophagy may be an increased accumulation of DPR proteins (Fig. 5e and Supplementary Fig. 7) which themselves have widely been proposed to contribute to neurodegeneration by (see review[47]): 1) sequestrating components of the ubiquitin-proteasome system (UPS), and compromising proteasome function, 2) binding to nucleocytoplasmic transport proteins and the central channel of the nuclear pore to impair nuclear pore trafficking, 3) altering phase separation of LCD-containing proteins and the dynamics of membrane-less organelles including stress granules, 4) restraining the access of translation factors to mRNA thereby blocking protein translation, 5) interfering with RNA splicing and nucleolar functions, 6) provoking DNA damage and genome instability, and 7) disrupting mitochondrial function(s). A recent *in vitro* study also reported that cellular clearance of overexpressed poly(PR)$_{50}$ was slowed in human iPSC-derived motor neurons with reduced C9ORF72, thereby contributing to accelerated neurodegeneration[34].

Protein homeostasis within post-mitotic neurons, especially motor neurons with large cell bodies and long axons, is critical to their long term survival, and is dependent on the protein chaperone machinery and key cellular clearance systems including UPS and autophagy[48]. Recognition of this and our evidence supporting the influence of C9ORF72 on autophagy in the CNS raises the possibility of converging disease mechanisms for ALS and FTD caused by a set of genes[35, 49] (*C9orf72*, *SQSTM1*, *UBQLN2*, *TBK1*, *OPTN*, *VCP*, *CHMP2B*, *FIG4* or *GRN*) each of which encode proteins that are directly or indirectly involved in autophagy-related protein clearance and membrane trafficking pathways. For instances of sporadic ALS, this also raises the possibility of a similar underlying mechanism with environmental factors or contributions from multiple gene variants leading to age-dependent inefficient clearance and disruption of protein quality control.

In mice, loss of C9ORF72 function predisposes animals to progressively-developed splenomegaly and lymphadenopathy and immune defects[17, 28, 29, 31]. However, there are a few sharp differences in the severity of disease reported by different groups, with some reporting premature death[17, 29, 31] and others not[28]. In our colony, homozygous *C9orf72* deletion produces early mortality in 100% of mice[17]. Similarly, Eggan and colleagues[31] reported that both heterozygous and homozygous deletion mice showed similar premature death. This contrasts with no premature deaths reported by Baloh and colleagues[28] in heterozygous or homozygous *C9orf72* deletion mice. This is all the more perplexing since each of these three *C9orf72* knockout lines were produced from the same targeted ES cells from the Knock Out Mouse Project (KOMP) Consortium and all are congenic in the C57BL6/J background. This discrepancy strongly suggests that external environmental factors, such as different animal housing conditions or different food (either of which may affect the microbiome), may underlie the differing phenotypes. It will be of future interest to determine how reduction in C9ORF72 can render cellular vulnerability to environmental insults, potentially altering the gut microbiome which has been linked to the pathogenesis of neurodegenerative diseases including Alzheimer's disease, Parkinson's disease and ALS[50].

Finally, in considering therapy development for C9ALS/FTD, our previous efforts have established that ASOs targeting the sequences adjacent to the hexanucleotide repeat in the first intron of the *C9orf72* pre-mRNA can direct RNase H-dependent degradation of repeat-

containing RNAs, without lowering the level of C9ORF72 protein encoding mRNAs[13, 17]. Our identification here of synergistic roles provided by gain-of-toxicity from repeat-containing RNAs and reduction in C9ORF72 function in mediating nervous system disease offers strong support for the rationale of the ASO approach targeting repeat-containing RNAs now in Phase I clinical trial.

METHODS

Animals

To generate mice expressing 450 repeat expansions with none, one or two alleles of endogenous *C9orf72* inactivated, *C9orf72* knockout mice were bred to BAC transgenic mice expressing 450 repeat expansions. Both the mouse strains were described previously[17] and were backcrossed to C57BL/6 for a minimum of six generations. The sex of animals was balanced in experiments. All experimental procedures were approved by the Institutional Animal Care and Use Committee of the University of California, San Diego.

Intracerebroventricular injections of AAV in neonatal mice

Generation of AAV vectors and neonatal viral injections were described previously[18]. Briefly, 2 or 66 repeats with 119 base pairs of the 5' flanking region and 100 base pairs of the 3' flanking region of the *C9orf72* gene were inserted into an adeno-associated virus (AAV) expression vector pAM/CBA-pl-WPRE-BGH containing inverted repeats of serotype 2. AAV particles were packaged into serotype 9 type capsid and purified. Pups from the mating between *C9orf72*$^{+/-}$ mice at post-natal day 0 were cryoanesthetized on ice until exhibiting no movement. A 32-gauge needle (Hamilton Company) was inserted at approximately two-fifths the distance between the lambda suture and each eye. Two microliters (1E10 genomes/μl) of AAV solution was manually injected into each cerebral ventricle.

Protein extraction and immunoblotting

Human or mouse CNS tissues were homogenized in standard RIPA lysis buffer and 30 μg of total protein lysate was resolved on a 10% SDS-PAGE. N-terminally His-tagged full length and short isoform (amino acid 1–222) C9ORF72 were expressed in Rosetta (DE3) bacteria and were purified with Ni-NTA beads (Qiagen) following the manufacturer's protocol. Proteins were transferred to nitrocellulose membranes and probed with antibodies against C9ORF72 (Proteintech, 1:1000), LC3B (Abcam, 1:1000), p62 (Novus,1:1000), Ubiquitin (Dako, 1:1000) and Actin (Abcam, 1:5000). The membranes were washed in PBS, with 0.1% Tween and blotted with primary antibodies. After the membrane was incubated with HRP-conjugated secondary antibody, bands were visualized by the ECL plus Western Blotting Detection System (Pierce).

RNA extraction and quantitative RT-PCR

Total RNA from mouse spinal cord, cerebellum, cortex and spleen was isolated with TRIZOL (Invitrogen) and first-strand complementary DNA (cDNA) was synthesized using the High-Capacity cDNA Reverse Transcription Kit (Thermo Fisher Scientific, Waltham, MA, USA). Quantitative RT-PCR reactions were conducted and analyzed on a CFX384

touch Real-time PCR machine (Bio-Rad). Human repeat-containing *C9orf72* RNAs were determined using Taqman real time-PCR. The level of human *C9orf72* transcripts were normalized to glyceraldehyde-3-phosphate dehydrogenase (Gapdh) or ATP synthase subunit beta mitochondrial precursor (Atp5b). Primers and probe sequences are listed in a previous study[17].

Transgene expression level in CNS samples from AAV-injected mice were determined using the SYBR Green supermix (Bio-Rad). Mouse ribosomal protein S9 (Rps9) gene was measured as standard genes. Primers sequences are listed as following: C9repeat Fwd = 5'AGCTTAGTACTCGCTGAGGGTG; C9repeat Rev = 5'GACTCCTGAGTTCCAGAGCTTG, as reported in a previous study[51].

Immunostaining

Sections from paraformaldehyde-fixed or formalin-fixed tissues were stained using protocols described previously[17] with antibodies against GFAP (Chemicon, 1:1000), Iba1 (Wako, 1:500), ChAT (Millipore, 1:300), poly(GA) (Rb4333, 1:1000), poly(GP) (Rb4335, 1:1000), poly(GR) (Rb4995, 1:1000), p62 (Novus, 1:200). Confocal images were acquired on a Nikon Eclipse Ti laser scanning confocal microscope using the Nikon EZ-C1 software.

Astrogliosis and microgliosis determined by GFAP or Iba1 fluorescence intensity

For quantification of GFAP and Iba1 staining, 10x images were taken and analyzed throughout each hippocampal region of mouse coronal brain sections using a Nikon Eclipse Ti microscope. Nikon Elements Software was used to subtract the background signals and determine the average fluorescence intensity (A.U.) across a region of interest. At least two sections from 4–5 mice were measured.

Quantification of lower motor neurons and hippocampal neurons

ChAT-positive ventral horn motor neurons were counted from 30 μm lumbar spinal cord cryosections, spaced 360 μm apart (15–30 sections per animal, minimum of three animals per genotype) and demonstrated as the average of total motor neurons counted divided by the number of sections.

Coronal brain OCT sections were immunostained with NeuN (GeneTex, 1:1000) and nuclei were stained with DAPI. Hippocampal CA1 region contains mainly NeuN-positive cells. For quantitation, DAPI-positive cells were counted in 3–5 consecutive sections manually by using the ImageJ software. Careful matching of the sections to compare similar anatomical regions was performed for each set of mice.

Poly(GP) and poly(GA) immunoassays

For poly(GP) and poly(GA) measurement, tissues were homogenized in 10% (w/v) buffer containing: 50 mM Tris, pH 7.4, 300 mM NaCl, 1% Triton X-100, 2% sodium dodecyl sulfate, 5 mM EDTA, as well as protease inhibitors. Homogenates were sonicated, centrifuged at 16,000 x g for 20 min and supernatants collected. The protein concentration of lysates was determined by bicinchoninic acid assay (Thermo Fisher Scientific). Poly(GP) levels in lysates were measured using a previously described sandwich immunoassay that

utilizes Meso Scale Discovery (MSD) electrochemiluminescence detection technology[52, 53]. Lysates from a given neuroanatomical region were diluted to the same concentration in Tris-buffered saline (TBS) and tested in duplicate wells. Serial dilutions of recombinant $(GP)_8$ in TBS were used to prepare the standard curve. Poly(GA) levels in lysates were similarly measured with an MSD-based poly(GA) sandwich immunoassay that employed a rabbit polyclonal poly(GA) antibody (Rb4333) and a mouse monoclonal poly(GA) antibody (clone 5F2)[53]. These antibodies specifically detect poly(GA). Poly(GA) levels in samples were interpolated from a standard curve prepared using recombinant $(GA)_{50}$.

Morphometric analysis and quantification of L5 root motor axons

Mice were perfused transcardially with 4% paraformaldehyde in 0.1 M Sorenson's phosphate buffer, pH 7.4. Roots from lumbar level 5 of the spinal cord (L5) were dissected from n > 3 animals per genotype at 12 months of age, and preserved in fixative at 4 °C until embedding. Roots were embedded in Epon-Araldite as previously described[54]. Thick sections (0.75 μm) were prepared and stained with toluidine blue for analysis by light microscopy. For animals in each group, cross sections of axons were analyzed using Image J software and axonal diameters were graphed as a size distribution curve.

Mouse ear fibroblast isolation and culture

Mouse ear fibroblasts (MEFs) were isolated and cultured from adult *C9orf72*$^{+/+}$, *C9orf72*$^{+/-}$ and *C9orf72*$^{-/-}$ mice as previously described[55]. MEFs were treated with either bafilomycin (Sigma) at 30 μM or rapamycin (Millipore) at 200 nM for 2 hours before analysis.

Embryonic stem cell (ESC) derived motor neuron culture

Mouse ESCs (Hb9::GFP) were purchased from ArunA Biomedical, and differentiated into motor neurons according to specifications provided by the manufacturer. ESCs were maintained and grown to 70–80% confluency in 6-well plates on top of a mouse embryonic fibroblast (iXCells Biotechnologies) layer prior to differentiation. To form embryoid bodies (EBs), cells were detached with 1 ml 0.25% Trypsin and resuspended in 10 ml motor neuron differentiation (Advance DMEM/F12: AB2 Basal medium (1:1), 10% knockout serum, 1% penicillin/streptomycin, 1% L-glutamine, and 2-mercaptoethanol). ESCs were plated at 1×10^6 cells per 10 cm on low-attachment Petri dishes. Day of seeding was defined as differentiation day 0. Medium was changed daily, and cultures were supplemented with retinoic acid (from day 1), purmorphamine (from day 1), and DAPT (from day 4). At differentiation day 6, the EBs were collected and washed in EBSS 3 times prior to dissociation into single cells using Papain (20U/ml, Worthington Biochemical Corporation)[56]. GFP+ motor neurons were sorted and seeded at 2000 – 3000 cells on top of wild type murine astrocyte layers per well in 96-well plates. Cells were treated with ASOs (10 μM) for 14 days and subjected to immunofluorescence staining. Briefly, cells were fixed in 4% PFA for 15 min, blocked in 5% BSA (made in 0.5% Triton X-100 in 0.1 M PBS) for 1 hour at room temperature and incubated with primary antibodies (NF-H, Abcam; SMI-32, Covance) in antibody diluent (CST) at 4°C overnight. The following day, cells were washed with 0.1 M PBS and incubated with fluorophore-conjugated secondary antibodies and DAPI at room temperature for 1 hr. Images from 20 fields per well were acquired using IC200-KIC (Vala Sciences) and analyzed using Acapella 2.6 (PekinElmer).

Mouse behavioral assays

Rotarod test—A Rota-rod Series 8 apparatus (Ugo Basille) was used. The rod was a knurled plastic dowel (6.0 cm diameter) set at a height of 30 cm and the latencies to fall were automatically recorded by a computer. During training the mice were placed on the stationary rotarod for 30 sec before the trial was initiated. Then each mouse was given 3 trials per day, with a 60 sec inter-trial interval on the accelerating rotarod (4–40 rpm over 5 min) for 5 consecutive days.

Locomotor activity—Locomotor activity was measured using an automated monitoring system (Kinder Associates, San Diego, CA). Polycarbonate cages (42 × 22 × 20 cm) containing a thin layer of bedding material were placed into frames (25.5 × 47 cm) mounted with photocell beams. Each mouse was tested for 60 min.

Grip strength—Grip strength was measured using a device consisting of a 10 cm long T-shaped bar connected to a digital dynamometer (Ugo Basile, Comerio, Italy). Mice were placed before the bar, which they usually grab spontaneously, and gently pulled backwards until they release the bar. Ten consecutive measurements were made for each animal and both the average and maximal readouts were recorded.

Gait analysis—Gait measures were collected using an automated gait analysis system (CatWalk [Noldus Instruments]). The mice were placed at one end of the runway and allowed to move to the other end of the runway, where they can enter a dark enclosure. The test was performed once a day for 5 days. Measurements include stride length (left and right) and stride width (front and back).

Barnes maze—The Barnes maze used was an opaque Plexiglas disc 75 cm in diameter elevated 58 cm above the floor by a tripod. Twenty holes, 5 cm in diameter, were located 5 cm from the perimeter, and a black Plexiglas escape box (19 × 8 × 7 cm) was placed under one of the holes. Distinct spatial cues were located all around the maze and were kept constant throughout the study. On the first day of testing, a training session was performed, which consists in leaving the mouse in the escape box for five minutes. One minute later, the first session was started. At the beginning of each session, the mouse was placed in the middle of the platform in a 10 cm high cylindrical black start chamber. After 10 sec the start chamber was removed, a light (400 lux) was turned on, and the mouse was allowed to freely explore the maze. The session ended when the mouse entered the escape tunnel or after 3 min elapsed. When the mouse entered the escape tunnel, the light was turned off and the mouse remained in the dark for one minute. When the mouse did not enter the tunnel by itself it was gently put in the escape box for one min. The tunnel was always located underneath the same hole (stable within the spatial environment), which was randomly determined for each mouse. Mice were tested once a day for 9 days.

Protein domain structure graphs

C9ORF72 protein domain structure graphs were prepared by MyDomains (https://prosite.expasy.org/mydomains).

Statistical analysis

All data were graphed and analyzed using Graphpad Prism 5. Group differences in each assay at each time point were analyzed by Student's *t*-test or one-way ANOVA or two-way ANOVA. No statistical methods were used to pre-determine sample sizes but our sample sizes are similar to those reported in previous publications[13,17]. Experiments were not randomized. Data distribution was assumed to be normal, but this was not formally tested. Data collection and analysis were not performed blind to the conditions of the experiments.

Reporting summary

Further information on research design is available in the Nature Research Reporting Summary linked to this article.

Data availability

The data that support the findings of this study are available from the corresponding author upon reasonable request.

Supplementary Material

Refer to Web version on PubMed Central for supplementary material.

ACKNOWLEDGMENTS

We thank Brian Myers, Marcus Maldonado, Jeesun Kim, Jaisen Lim, Jean Yasis, Drs. Charles J. Heyser, Dara Ditsworth, Kent Osborn, Jeannie Chew for their advice and technical assistance. We thank Drs. Martin Fugere and Brian Kaspar at AveXis for providing help in sorting mouse ESC-derived motor neurons. We thank Ionis Pharmaceuticals for providing ASOs. We thank all members of the D.W.C., C.L.-T., J.R. and S.D.C. groups for critical suggestions on this project. We apologize to those whose prior work we have not been able to cite in order to comply with editorial limit on the number of citations. This work was supported by grants from NINDS/NIH R01-NS27036 to D.W.C. and S.D.C. and R01-NS087227 to C.L.-T.; from the NIA/NIH-supported UCSD Alzheimer's Disease Research Center to C.L.-T. and D.W.C.; from Target ALS to C.L.-T. and J.R.; from NINDS/NIH R35-NS097273, P01-NS084974 and R01-NS088689 to L.P.; from P01-NS099114 to T.G. and L.P.; from Target ALS to T.G., L.P. and Y.Z.. C.L.-T is the recipient of the Healey Family ALS Endowed Chair for Research. Q.Z. was recipient of a Milton Safenowitz Postdoctoral fellowship and a STARTER grant from the ALS Association. J.J. was recipient of a Career Development grant from the Muscular Dystrophy Association (MDA #479769).

REFERENCES

1. DeJesus-Hernandez M, et al. Expanded GGGGCC hexanucleotide repeat in noncoding region of C9ORF72 causes chromosome 9p-linked FTD and ALS. Neuron 72, 245–256 (2011). [PubMed: 21944778]
2. Renton AE, et al. A hexanucleotide repeat expansion in C9ORF72 is the cause of chromosome 9p21-linked ALS-FTD. Neuron 72, 257–268 (2011). [PubMed: 21944779]
3. Levine TP, Daniels RD, Gatta AT, Wong LH & Hayes MJ The product of C9orf72, a gene strongly implicated in neurodegeneration, is structurally related to DENN Rab-GEFs. Bioinformatics 29, 499–503 (2013). [PubMed: 23329412]
4. Zu T, et al. Non-ATG-initiated translation directed by microsatellite expansions. Proceedings of the National Academy of Sciences of the United States of America 108, 260–265 (2011). [PubMed: 21173221]
5. Zu T, et al. RAN proteins and RNA foci from antisense transcripts in C9ORF72 ALS and frontotemporal dementia. Proceedings of the National Academy of Sciences of the United States of America 110, E4968–4977 (2013). [PubMed: 24248382]

6. Mori K, et al. Bidirectional transcripts of the expanded C9orf72 hexanucleotide repeat are translated into aggregating dipeptide repeat proteins. Acta neuropathologica 126, 881–893 (2013). [PubMed: 24132570]
7. Ash PE, et al. Unconventional translation of C9ORF72 GGGGCC expansion generates insoluble polypeptides specific to c9FTD/ALS. Neuron 77, 639–646 (2013). [PubMed: 23415312]
8. Balendra R & Isaacs AM C9orf72-mediated ALS and FTD: multiple pathways to disease. Nat Rev Neurol 14, 544–558 (2018). [PubMed: 30120348]
9. Mackenzie IR, et al. Quantitative analysis and clinico-pathological correlations of different dipeptide repeat protein pathologies in C9ORF72 mutation carriers. Acta neuropathologica 130, 845–861 (2015). [PubMed: 26374446]
10. Li N & Lagier-Tourenne C Nuclear pores: the gate to neurodegeneration. Nat Neurosci 21, 156–158 (2018). [PubMed: 29371653]
11. Saberi S, et al. Sense-encoded poly-GR dipeptide repeat proteins correlate to neurodegeneration and uniquely co-localize with TDP-43 in dendrites of repeat-expanded C9orf72 amyotrophic lateral sclerosis. Acta Neuropathol 135, 459–474 (2018). [PubMed: 29196813]
12. Mackenzie IR, et al. Dipeptide repeat protein pathology in C9ORF72 mutation cases: clinico-pathological correlations. Acta neuropathologica 126, 859–879 (2013). [PubMed: 24096617]
13. Lagier-Tourenne C, et al. Targeted degradation of sense and antisense C9orf72 RNA foci as therapy for ALS and frontotemporal degeneration. Proceedings of the National Academy of Sciences of the United States of America 110, E4530–4539 (2013). [PubMed: 24170860]
14. Wojciechowska M & Krzyzosiak WJ Cellular toxicity of expanded RNA repeats: focus on RNA foci. Hum Mol Genet 20, 3811–3821 (2011). [PubMed: 21729883]
15. Haeusler AR, Donnelly CJ & Rothstein JD The expanding biology of the C9orf72 nucleotide repeat expansion in neurodegenerative disease. Nat Rev Neurosci 17, 383–395 (2016). [PubMed: 27150398]
16. Burguete AS, et al. GGGGCC microsatellite RNA is neuritically localized, induces branching defects, and perturbs transport granule function. Elife 4, e08881 (2015). [PubMed: 26650351]
17. Jiang J, et al. Gain of Toxicity from ALS/FTD-Linked Repeat Expansions in C9ORF72 Is Alleviated by Antisense Oligonucleotides Targeting GGGGCC-Containing RNAs. Neuron 90, 535–550 (2016). [PubMed: 27112497]
18. Liu Y, et al. C9orf72 BAC Mouse Model with Motor Deficits and Neurodegenerative Features of ALS/FTD. Neuron 90, 521–534 (2016). [PubMed: 27112499]
19. Chew J, et al. Neurodegeneration. C9ORF72 repeat expansions in mice cause TDP-43 pathology, neuronal loss, and behavioral deficits. Science 348, 1151–1154 (2015). [PubMed: 25977373]
20. Belzil VV, et al. Reduced C9orf72 gene expression in c9FTD/ALS is caused by histone trimethylation, an epigenetic event detectable in blood. Acta neuropathologica 126, 895–905 (2013). [PubMed: 24166615]
21. Donnelly CJ, et al. RNA toxicity from the ALS/FTD C9ORF72 expansion is mitigated by antisense intervention. Neuron 80, 415–428 (2013). [PubMed: 24139042]
22. Frick P, et al. Novel antibodies reveal presynaptic localization of C9orf72 protein and reduced protein levels in C9orf72 mutation carriers. Acta Neuropathol Commun 6, 72 (2018). [PubMed: 30075745]
23. Waite AJ, et al. Reduced C9orf72 protein levels in frontal cortex of amyotrophic lateral sclerosis and frontotemporal degeneration brain with the C9ORF72 hexanucleotide repeat expansion. Neurobiol Aging 35, 1779 e1775–1779 e1713 (2014).
24. Xi Z, et al. Hypermethylation of the CpG island near the G4C2 repeat in ALS with a C9orf72 expansion. Am J Hum Genet 92, 981–989 (2013). [PubMed: 23731538]
25. Xi Z, et al. The C9orf72 repeat expansion itself is methylated in ALS and FTLD patients. Acta neuropathologica 129, 715–727 (2015). [PubMed: 25716178]
26. Ciura S, et al. Loss of function of C9orf72 causes motor deficits in a zebrafish model of amyotrophic lateral sclerosis. Ann Neurol 74, 180–187 (2013). [PubMed: 23720273]
27. Therrien M, Rouleau GA, Dion PA & Parker JA Deletion of C9ORF72 results in motor neuron degeneration and stress sensitivity in C. elegans. PLoS One 8, e83450 (2013). [PubMed: 24349511]

28. O'Rourke JG, et al. C9orf72 is required for proper macrophage and microglial function in mice. Science 351, 1324–1329 (2016). [PubMed: 26989253]
29. Atanasio A, et al. C9orf72 ablation causes immune dysregulation characterized by leukocyte expansion, autoantibody production, and glomerulonephropathy in mice. Scientific reports 6, 23204 (2016). [PubMed: 26979938]
30. Ugolino J, et al. Loss of C9orf72 Enhances Autophagic Activity via Deregulated mTOR and TFEB Signaling. PLoS genetics 12, e1006443 (2016). [PubMed: 27875531]
31. Burberry A, et al. Loss-of-function mutations in the C9ORF72 mouse ortholog cause fatal autoimmune disease. Sci Transl Med 8, 347ra393 (2016).
32. Sullivan PM, et al. The ALS/FTLD associated protein C9orf72 associates with SMCR8 and WDR41 to regulate the autophagy-lysosome pathway. Acta Neuropathol Commun 4, 51 (2016). [PubMed: 27193190]
33. Koppers M, et al. C9orf72 ablation in mice does not cause motor neuron degeneration or motor deficits. Ann Neurol 78, 426–438 (2015). [PubMed: 26044557]
34. Shi Y, et al. Haploinsufficiency leads to neurodegeneration in C9ORF72 ALS/FTD human induced motor neurons. Nat Med 24, 313–325 (2018). [PubMed: 29400714]
35. Sellier C, et al. Loss of C9ORF72 impairs autophagy and synergizes with polyQ Ataxin-2 to induce motor neuron dysfunction and cell death. The EMBO journal 35, 1276–1297 (2016). [PubMed: 27103069]
36. Yang M, et al. A C9ORF72/SMCR8-containing complex regulates ULK1 and plays a dual role in autophagy. Sci Adv 2, e1601167 (2016). [PubMed: 27617292]
37. Webster CP, et al. The C9orf72 protein interacts with Rab1a and the ULK1 complex to regulate initiation of autophagy. The EMBO journal 35, 1656–1676 (2016). [PubMed: 27334615]
38. Zhang Y, et al. The C9orf72-interacting protein Smcr8 is a negative regulator of autoimmunity and lysosomal exocytosis. Genes Dev 32, 929–943 (2018). [PubMed: 29950492]
39. Ho WY, et al. The ALS-FTD-linked gene product, C9orf72, regulates neuronal morphogenesis via autophagy. Autophagy, 1–16 (2019).
40. Liu EY, et al. C9orf72 hypermethylation protects against repeat expansion-associated pathology in ALS/FTD. Acta neuropathologica 128, 525–541 (2014). [PubMed: 24806409]
41. Zhang D, Iyer LM, He F & Aravind L Discovery of Novel DENN Proteins: Implications for the Evolution of Eukaryotic Intracellular Membrane Structures and Human Disease. Frontiers in genetics 3, 283 (2012). [PubMed: 23248642]
42. Scholz J, Niibori Y, P WF & J PL Rotarod training in mice is associated with changes in brain structure observable with multimodal MRI. Neuroimage 107, 182–189 (2015). [PubMed: 25497397]
43. Nixon RA, Yang DS & Lee JH Neurodegenerative lysosomal disorders: a continuum from development to late age. Autophagy 4, 590–599 (2008). [PubMed: 18497567]
44. Klionsky DJ, et al. Guidelines for the use and interpretation of assays for monitoring autophagy (3rd edition). Autophagy 12, 1–222 (2016). [PubMed: 26799652]
45. Ciechanover A The ubiquitin-proteasome proteolytic pathway. Cell 79, 13–21 (1994). [PubMed: 7923371]
46. Chitiprolu M, et al. A complex of C9ORF72 and p62 uses arginine methylation to eliminate stress granules by autophagy. Nat Commun 9, 2794 (2018). [PubMed: 30022074]
47. Jiang J & Ravits J Pathogenic Mechanisms and Therapy Development for C9orf72 Amyotrophic Lateral Sclerosis/Frontotemporal Dementia. Neurotherapeutics 16, 1115–1132 (2019). [PubMed: 31667754]
48. Nassif M, Woehlbier U & Manque PA The Enigmatic Role of C9ORF72 in Autophagy. Front Neurosci 11, 442 (2017). [PubMed: 28824365]
49. Taylor JP, Brown RH Jr. & Cleveland DW Decoding ALS: from genes to mechanism. Nature 539, 197–206 (2016). [PubMed: 27830784]
50. Roy Sarkar S & Banerjee S Gut microbiota in neurodegenerative disorders. J Neuroimmunol 328, 98–104 (2019). [PubMed: 30658292]

METHODS-ONLY REFERENCES

51. Kramer NJ, et al. Spt4 selectively regulates the expression of C9orf72 sense and antisense mutant transcripts. Science 353, 708–712 (2016). [PubMed: 27516603]
52. Su Z, et al. Discovery of a biomarker and lead small molecules to target r(GGGGCC)-associated defects in c9FTD/ALS. Neuron 83, 1043–1050 (2014). [PubMed: 25132468]
53. Gendron TF, et al. Cerebellar c9RAN proteins associate with clinical and neuropathological characteristics of C9ORF72 repeat expansion carriers. Acta neuropathologica 130, 559–573 (2015). [PubMed: 26350237]
54. Parone PA, et al. Enhancing mitochondrial calcium buffering capacity reduces aggregation of misfolded SOD1 and motor neuron cell death without extending survival in mouse models of inherited amyotrophic lateral sclerosis. J Neurosci 33, 4657–4671 (2013). [PubMed: 23486940]
55. Shao C, et al. Mitotic recombination produces the majority of recessive fibroblast variants in heterozygous mice. Proceedings of the National Academy of Sciences of the United States of America 96, 9230–9235 (1999). [PubMed: 10430925]
56. Jiang LL, et al. Membralin deficiency dysregulates astrocytic glutamate homeostasis leading to ALS-like impairment. J Clin Invest 129, 3103–3120 (2019). [PubMed: 31112137]

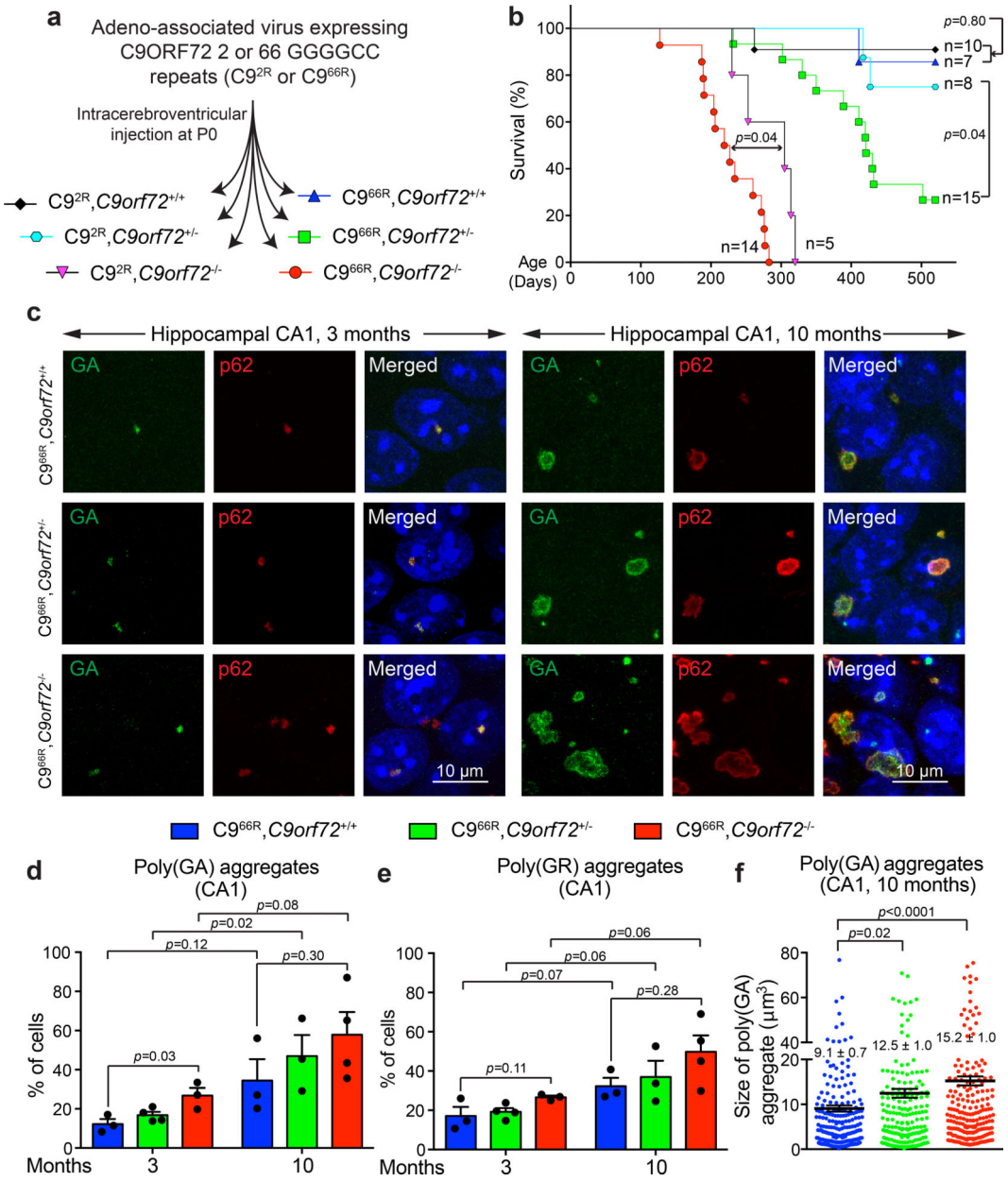

Figure 1: Reduction or loss of C9ORF72 in mice expressing 66 GGGGCC repeats induces or accelerates, respectively, premature death and leads to increased dipeptide-repeat protein accumulation.

(a) Schematic of intracerebroventricular injection of C9AAV in P0 mice to produce cohorts of mice expressing 2 or 66 GGGGCC repeats with neither, one or both endogenous *C9orf72* alleles inactivated ($C9^{2R}$,*C9orf72*$^{+/+}$; $C9^{2R}$,*C9orf72*$^{+/-}$; $C9^{2R}$,*C9orf72*$^{-/-}$; $C9^{66R}$,*C9orf72*$^{+/+}$; $C9^{66R}$,*C9orf72*$^{+/-}$; $C9^{66R}$,*C9orf72*$^{-/-}$).

(b) Survival curve (up to 520 days) of the mouse cohorts in **(a)**. Statistical evaluation using the Gehan-Breslow-Wilcoxon test.

(c) Representative images of poly(GA) aggregates or p62 in the hippocampal CA1 region of (*left*) 3- or (*right*) 10-month-old mice expressing 66 GGGGCC repeats with normal,

reduced, or no endogenous C9ORF72. Experiment was reproduced three times independently with similar results.

(d-e) Percentage of cells with detectable poly(GA) **(d)** or poly(GR) **(e)** in the cortex of 3- and 10-month-old mice expressing 66 GGGGCC repeats with normal, reduced or absence of endogenous C9ORF72. Error bars represent SEM (for 3-month-old animals, n = 3 $C9^{66R}$,*C9orf72*$^{+/+}$, n = 4 $C9^{66R}$,*C9orf72*$^{+/-}$, n = 3 $C9^{66R}$,*C9orf72*$^{-/-}$; for 10-month-old animals, n = 3 $C9^{66R}$,*C9orf72*$^{+/+}$, n = 3 $C9^{66R}$,*C9orf72*$^{+/-}$, n = 4 $C9^{66R}$,*C9orf72*$^{-/-}$; over 80 cells counted per animal). Between different groups of genotypes, statistical evaluations were performed using one-way ANOVA with Tukey's post hoc test. Between different groups of ages within the same genotype, statistical evaluations were performed using student's *t*-test, unpaired, two-tailed.

(f) Aggregate size of poly(GA) aggregates in the hippocampal CA1 region of 10-month-old mice expressing 66 GGGGCC repeats with normal, reduced, or absence of endogenous C9ORF72. Each dot represents the size of a poly(GA) aggregate (n = 3 animals per group). Error bars represent SEM. Statistical evaluations were performed using one-way ANOVA with Tukey's post hoc test.

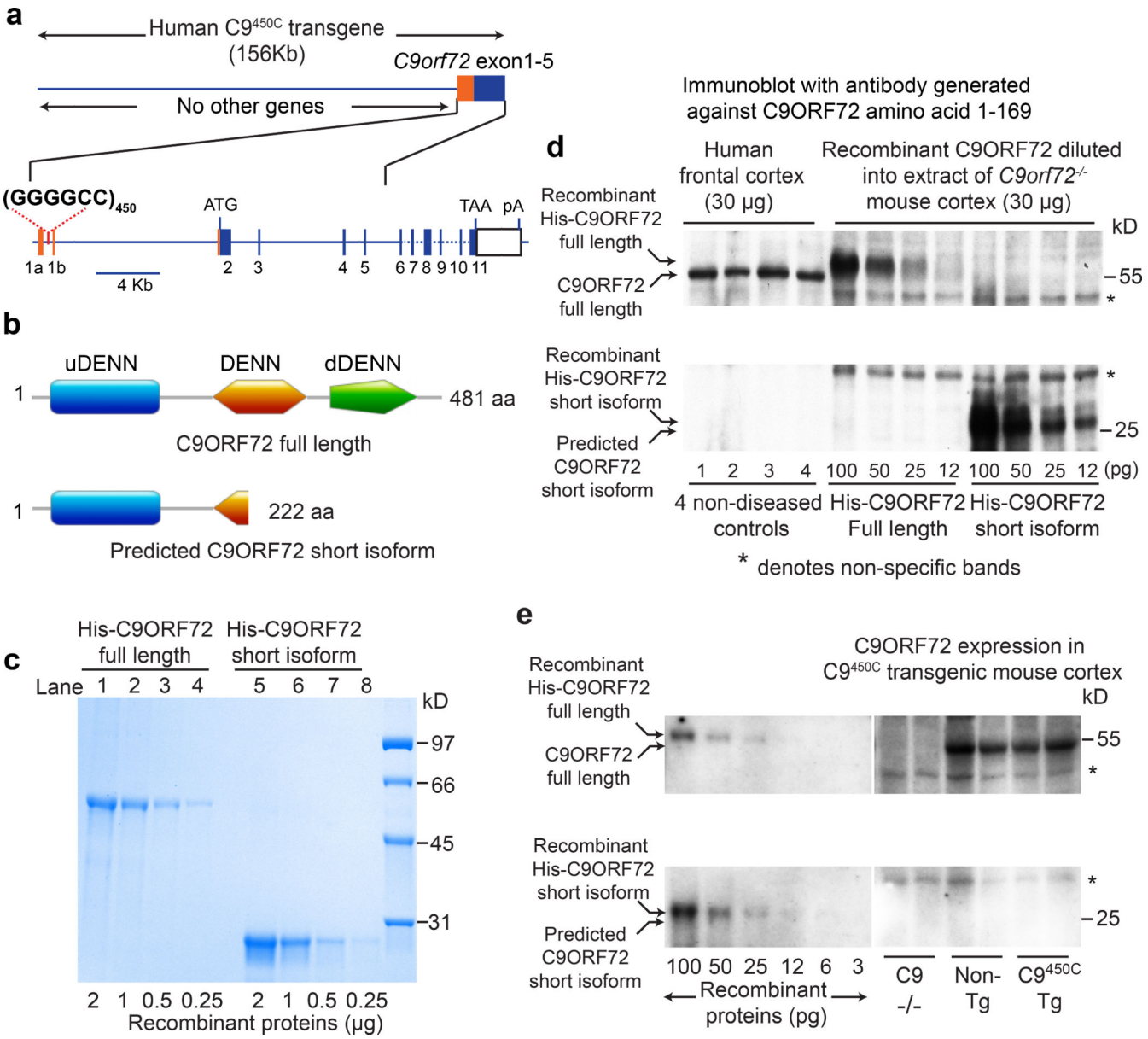

Figure 2: No detection of a predicted C9ORF72 short-isoform protein in frontal cortex from human samples or C9^{450C} transgenic mice.

(a) Schematic of the portion of the *C9orf72* gene included in *C9orf72* BAC transgenic mice with 450 hexanucleotide repeats.

(b) Domains of C9ORF72 full length (481 amino acids, 54 kD) and predicted short isoform (222 amino acids, 25 kD) protein. DENN, differentially expressed in neoplastic versus normal cells; uDENN, upstream DENN; dDENN, downstream DENN.

(c) Purified his-tagged full length (lanes 1–4) and predicted short isoform (lanes 5–8) C9ORF72 recombinant proteins analyzed by Coomassie staining of a SDS-polyacrylamide gel.

(d) Immunoblot testing for the presence of the predicted C9ORF72 short isoform in normal human cortex, visualized with antibodies generated against the human C9ORF72 N-

terminus (amino acids 1–169). Quantitation standards were produced through immunoblots with decreasing amounts (from 100 to 12 pg) of His-tagged full length or short isoform recombinant proteins diluted into extracts of *C9orf72*$^{-/-}$ mice (30 μg). Two independent experiments were performed with similar results.

(e) Immunoblot testing for the presence of the predicted C9ORF72 short isoform in cortical extracts from transgenic C9^{450} mice, using quantification standards as in **(d)**. Three independent experiments were performed with similar results.

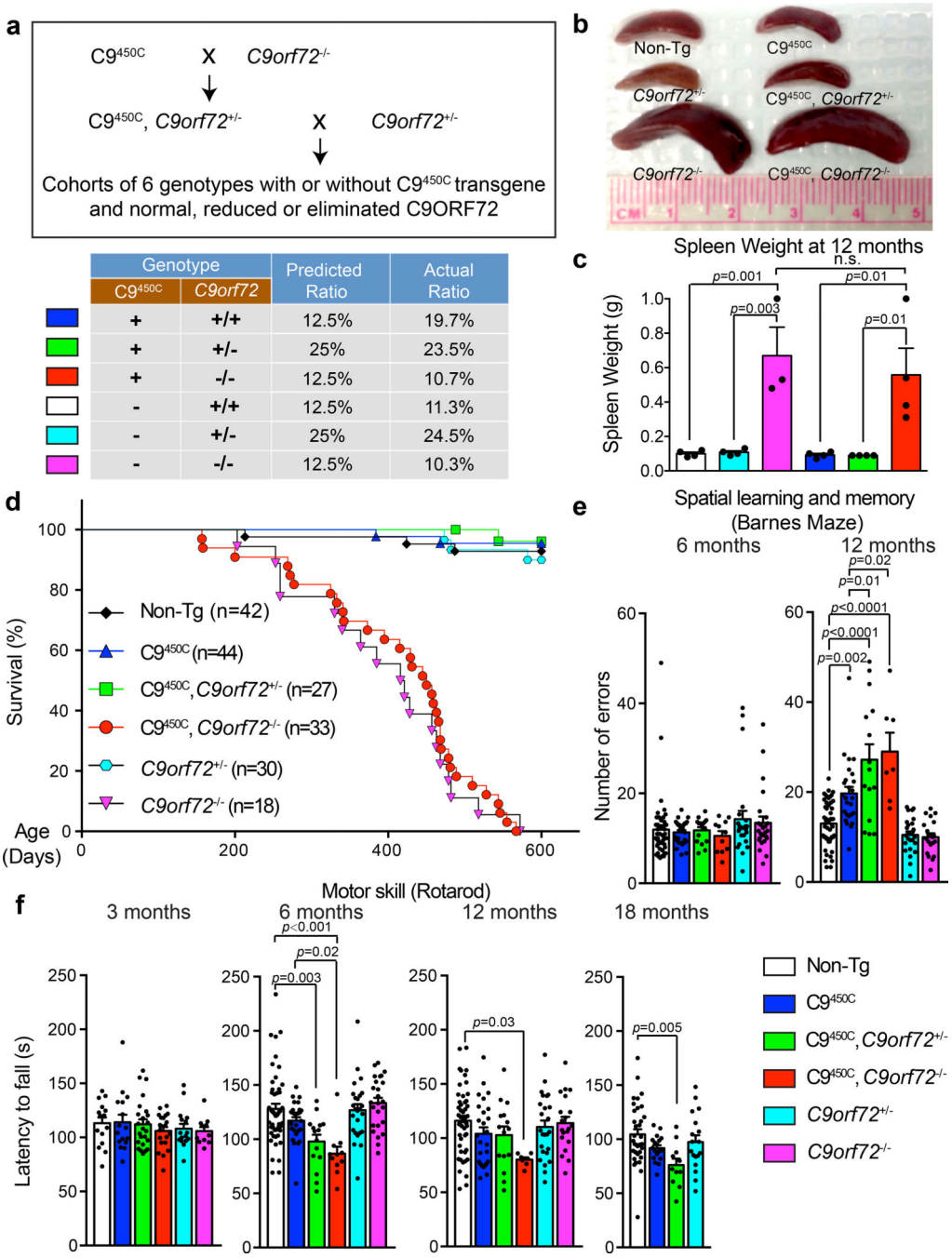

Figure 3: Reduction or loss of endogenous C9ORF72 exacerbates age-dependent cognitive abnormalities and motor deficits in C9^{450C} mice.

(a) Schematic of the breeding strategy to produce *C9orf72* transgenic mice with normal, reduced or absence of endogenous C9ORF72, including the predicted ratios for Mendelian inheritance of each genotype and observed ratios in the breeding cohorts.

(b) Spleen sizes at 12 months of age for mice with indicated genotypes. Experiment was reproduced three times independently with similar results.

(c) Spleen weight at 12 months of age. Error bars represent SEM (n = 4 Non-Tg, n = 4 *C9orf72*$^{+/-}$, n = 3 *C9orf72*$^{-/-}$, n = 4 C9^{450C}, n = 4 C9^{450C},*C9orf72*$^{+/-}$, n = 4 C9^{450C},*C9orf72*$^{-/-}$). Statistical significance assessed with one-way ANOVA with Tukey's post hoc test. n.s., not significant.

(d) Survival curve up to 600 days for mice with indicated genotypes.

(e-f) Behavioral performance in *C9orf72* transgenic mice with normal, reduced or absence of C9ORF72 (n = 49 [Non-Tg], n = 28 C9^{450C}, n = 15 C9^{450C},*C9orf72*$^{+/-}$, n = 11 C9^{450C},*C9orf72*$^{-/-}$, n = 25 *C9orf72*$^{+/-}$, n = 25 *C9orf72*$^{-/-}$). **(e)** Spatial learning and memory performance on a Barnes maze at 6 and 12 months of age showing the number of errors in finding the escape chamber at days 7–9. **(f)** Motor performance on a rotarod measured by the latency to fall at 6, 12 and 18 months of age. A separate cohort of *C9orf72* transgenic mice with normal, reduced, or absence of endogenous C9ORF72 (n = 15 Non-Tg, n = 16 C9^{450C}, n = 24 C9^{450C},*C9orf72*$^{+/-}$, n = 21 C9^{450C},*C9orf72*$^{-/-}$, n = 16 *C9orf72*$^{+/-}$, n = 11 *C9orf72*$^{-/-}$) was tested at 3 months of age. Error bars represent SEM. Statistical evaluations were performed using one-way ANOVA with Tukey's post hoc test.

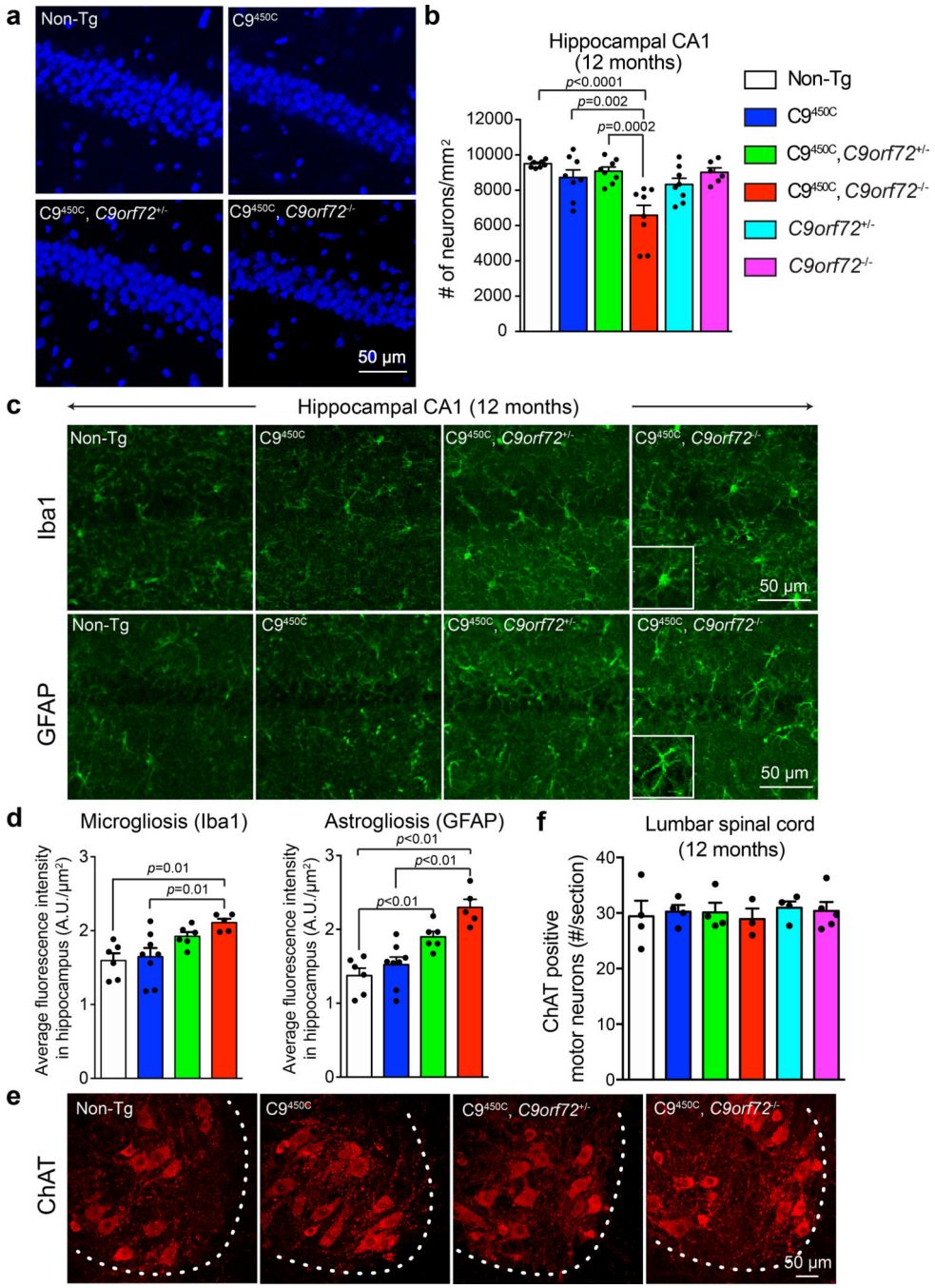

Figure 4: Loss of C9ORF72 promotes degeneration of hippocampal neurons and glial activation in C9^{450C} transgenic mice.

(a-b) Representative images **(a)** and quantification **(b)** of DAPI-positive nuclei in the hippocampal CA1 region in 12-month-old *C9orf72* transgenic mice with reduced or loss of endogenous C9ORF72. Each solid dot represents a CA1 region from one hemisphere (n = 4 Non-Tg, n = 4 C9^{450C}, n = 4 C9^{450C},*C9orf72*$^{+/-}$, n = 4 C9^{450C},*C9orf72*$^{-/-}$, n = 4 *C9orf72*$^{+/-}$, n = 3 *C9orf72*$^{-/-}$). Error bars represent SEM. Statistical evaluations were performed using one-way ANOVA with Tukey's post hoc test.

(c-d) Representative images **(c)** and quantification **(d)** of immunofluorescence staining with antibodies recognizing the microglial marker Iba-1 (*upper panels*) and the astrocytic marker GFAP (*lower panels*) in the hippocampal region of 12-month-old *C9orf72* transgenic mice with normal, reduced, or absence of endogenous C9ORF72. Each solid dot represents a hippocampal region from one hemisphere per animal (n = 3 Non-Tg, n = 4 $C9^{450C}$, n = 3 $C9^{450C}$,$C9orf72^{+/-}$, n = 3 $C9^{450C}$,$C9orf72^{-/-}$). Error bars represent SEM. Statistical evaluations were performed using one-way ANOVA with Tukey's post hoc test.
(e) Choline acetyltransferase (ChAT)-positive motor neurons detected by immunofluorescence in the anterior horn of lumbar spinal cords of *C9ORF72* transgenic mice with reduced or loss of endogenous C9ORF72 at 12 months of age.
(f) Average number of ChAT-positive motor neurons per section from lumbar spinal cords at 12 months of age. Error bars represent SEM (n = 4–5 animals per group). Statistical evaluations were performed using one-way ANOVA with Tukey's post hoc test.

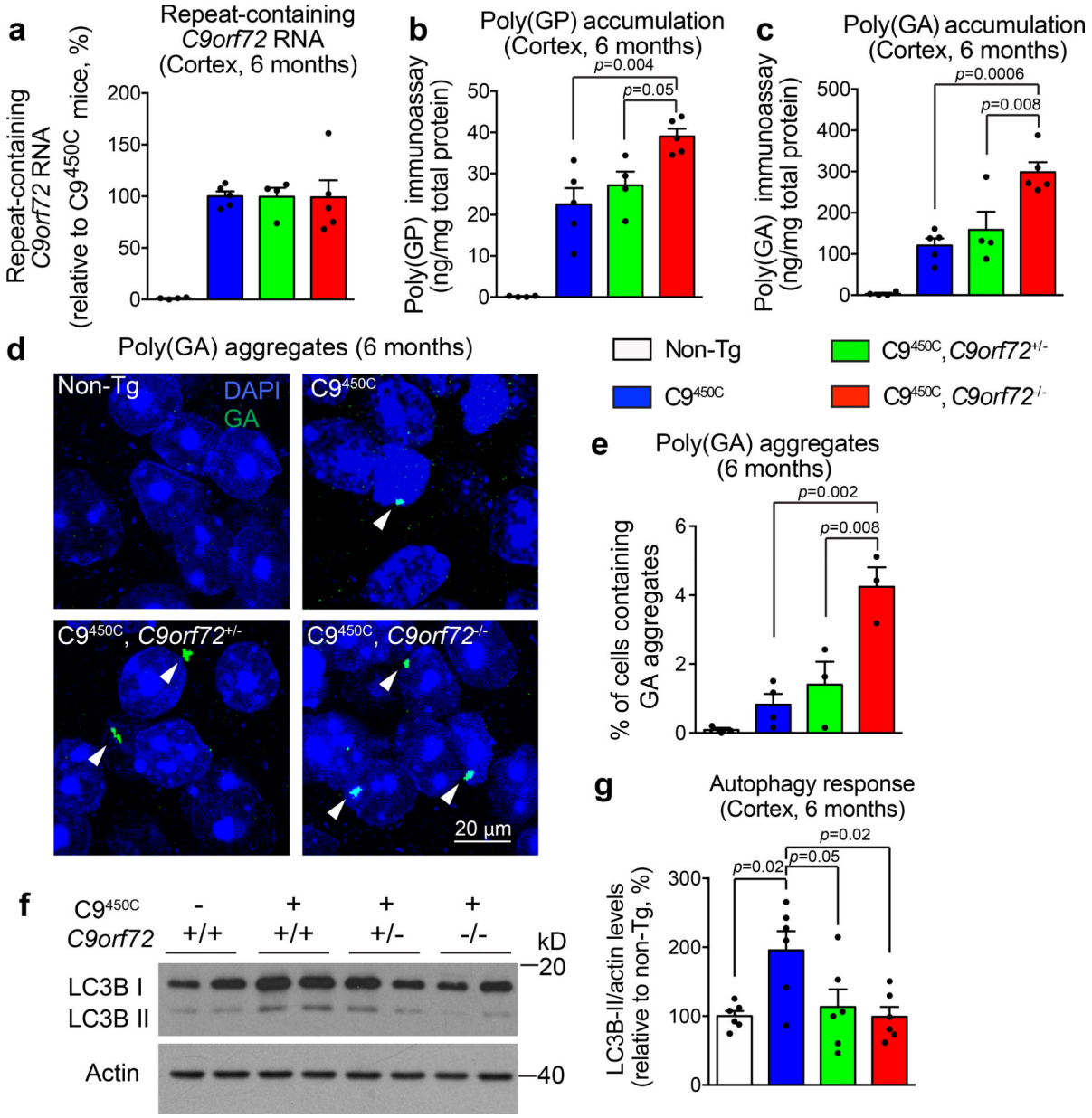

Figure 5: Loss of endogenous C9ORF72 inhibits autophagy accompanied by increased accumulation of polydipeptides produced by AUG-independent translation in C9^{450C} transgenic mice.

(a) Repeat-containing *C9orf72* RNA expression in the cortex of *C9orf72* transgenic mice with normal, reduced, or absence of endogenous C9ORF72 at 6 months of age. Error bars represent SEM (n = 4 Non-Tg, n = 5 C9^{450C}], n = 4 C9^{450C},*C9orf72*$^{+/-}$, n = 5 C9^{450C},*C9orf72*$^{-/-}$).

(b-c) Levels of poly(GP) **(b)** and poly(GA) **(c)** by immunoassay in the cortical extracts of *C9ORF72* transgenic mice with normal, reduced, or absence of C9ORF72 at 6 months of age. Error bars represent SEM (n = 4 Non-Tg, n = 5 C9^{450C}, n = 4 C9^{450C},*C9orf72*$^{+/-}$, n = 5 C9^{450C},*C9orf72*$^{-/-}$). Statistical analyses were performed using one-way ANOVA with Tukey's post hoc test.

(d-e) Representative images **(d)** and quantification **(e)** of poly(GA) aggregates in the retrosplenial granular cortex of *C9orf72* transgenic mice with normal, reduced or absence of C9ORF72 at 6 months of age. White arrowheads indicate poly(GA) aggregates. Error bars represent SEM (n = 3 Non-Tg, n = 4 $C9^{450C}$, n = 3 $C9^{450C}$,$C9orf72^{+/-}$, n = 3 $C9^{450C}$,$C9orf72^{-/-}$). Statistical analyses were performed using one-way ANOVA with Tukey's post hoc test.

(f-g) Immunoblotting analyses of cortical extracts from 6-month-old *C9orf72* transgenic mice with reduced or loss of C9ORF72 visualized with antibodies to the autophagic marker LC3 **(f)**. Actin was used as a loading control. Quantification of LC3B-II accumulated levels were normalized to actin **(g).** Error bars represent SEM (n = 6 per group). Statistical analyses were performed using one-way ANOVA with Tukey's post hoc test.